Computational Condensed Matter 35 (2023) e00803

Contents lists available at ScienceDirect

Computational Condensed Matter

journal homepage: www.elsevier.com/locate/cocom

Effect of Cu doping on structural, electronic and thermoelectric properties of double perovskite Cs_2NaVCl_6

Mohsen Doust Mohammadi [a], Syed Zuhair Abbas Shah [b,e,*], Hitler Louis [c], Tomsmith O. Unimuke [c], Gideon E. Mathias [c], Fahim Ahmed [d]

[a] School of Chemistry, College of Science, University of Tehran, Tehran, 14176, Iran
[b] Department of Physics, Thal University, Bhakkar, 30000, Pakistan
[c] Computational and Bio-Simulation Research Group, University of Calabar, Calabar, Nigeria
[d] Department of Physics, Division of Science and Technology, University of Education, Lahore, 54000, Pakistan
[e] Institute of Physics, Gomal University, D.I. Khan, 29050, Pakistan

ARTICLE INFO

Keywords:
Density functional theory
Seebeck coefficient
Thermal conductivity
Double perovskite
High absorption coefficient
Semiconductors
Solar cell materials
Thermoelectric materials

ABSTRACT

Double halide perovskite constitutes an interesting class of eco-friendly, and stable materials with significant potential as efficient energy harvesting materials. Their simple crystalline packing and tunability offers substantial advantage. Herein, the structural, electronic, and thermoelectric attributes of percentage Cu doped double perovskite (Cs_2NaVCl_6) is explored with the quantum espresso code within the framework of density functional theory using the generalized gradient approximation (GGA-PBE) with ultra-soft pseudopotential for the inherent atoms. Electronic and thermoelectric properties were all achieved via the GGA + U method to accurately compute the band gap and similar properties. The results express an inverse relationship between the lattice parameters and band gap. The lattice parameters increased with the increase in doping percentage. Similarly, the conductivity of the studied perovskite increased considerably with the increase in the percentage dopant. The calculated band gap was observed within the range of 1.7 eV–1.2 eV decreasing considerably with the increase in percentage doping and therefore suggesting an increase in the conductivity and other thermoelectric properties of the engineered perovskite material. However, the equilibrium lattice constants in accordance with the percentage doping reveal that the higher the percentage doping, the higher the equilibrium lattice constant. This inferred that 25% endohedral replacements of vanadium atoms by copper atoms give the best perovskite material owing to the fact that when the lattice constant increases with a corresponding decrease in the value of modulus of elasticity, there is a decrease in the stability of the perovskite material.

1. Introduction

Solar-based energy is a good source of economical energy which has the capability of giving a spotless stockpile of energy and is advanced as one of the primary innovations with the potential to provide a clean energy supply and address the current and upcoming energy crises [1,2] Perovskite solar cells (PSCs) have come into the spotlight recently [3,4] with extremely promising characteristics like little transport effective masses, long charge dissemination lengths, high charge transport versatility and high power conversion efficiencies (PCE) [5–7] and equivalent to the perceived CIGS and Cadmium telluride (CdTe) solar based cells [8]. There have been different degrees of transformation proficiency rates for novel perovskite materials with the most remarkable realized rate being 25.2% [8]. Moreover, perovskite solar cells are designed by incorporating mainly ample elements and can be set up utilizing a scope of unique wet-synthetic and vacuum-based methods, which empowers minimal expense production [5,6]. They have the best-ever PCE overhaul rate among all solar-based technologies examined up to this point and have been believed to be the "next ultimate thing in photovoltaics" [1,7]. This belief is coordinated by their high absorption coefficient, legitimate band gap, balanced electron, and hole mobility as well as low inborn recombination rates [8].

Methyl ammonium lead halide perovskite (MALHP) has evolved as one of the most significant model complexes for the perovskite solar cells adopting the general perovskite configuration of ABX_3 [9]. The dipolar MA^+ cations possess enormous cuboctahedral interstitial space between

* Corresponding author. Department of Physics, Thal University, Bhakkar, 30000, Pakistan.
E-mail address: Zuhair.abbas@uos.edu.pk (S.Z.A. Shah).

https://doi.org/10.1016/j.cocom.2023.e00803
Received 24 November 2022; Received in revised form 23 March 2023; Accepted 23 March 2023
Available online 25 March 2023

the organized B cation of Pb_2^+ and the six iodides (X) [10]. This model complex has been explored in high-proficiency solar-based cells and lasing applications as LEDs [11,12] among others. Nevertheless, persistent issues relating to device stability and natural uncertainties with respect to lead toxicity have made conceivable the probability of cationic exchange and blended halogen exchange which permits the tuning of PSC electronic structure [13,14], has animated a ton of hypothetical and exploratory research outfitted towards the grasping and total comprehension of the material architecture and physics within these frameworks. Lead replacement with other metals is a huge topic intended to meet natural worries and furthermore invigorate a change to more complex perovskite crystal structures. There are different productive instances of perovskite materials that are viewed as another class in the perovskite solar cell materials family with low toxicity, structural stability, and tenability [15]. Recently, indium-based DPs Cs_2InAgX_6 (X = Cl, Br, I) were explored as suitable materials for optoelectronic and thermoelectric applications. These findings demonstrate that these materials had considerable inherent attributes suited for optical and thermoelectric applications as non-traditional energy harvesting devices [16–18]. Also, the efficacy of $Cs_2InAgCl_6$ double perovskite material has been evaluated and reported by Volonakis et al. Both experimental and computational calculations were performed on a set of halogens functionalized $Cs_2InAgCl_6$ derivatives. The authors recorded a remarkable direct band gap of 3.3 eV and observed that functionalization with halogen significantly improves the band gaps and subsequent suitability as double perovskite solar materials [19]. Moreso, ab-initio methods were utilized to envisage the inherent optoelectronic properties of organic halide-based double perovskite materials formulated by $(CH_3NH_3)_2$) $AgMBr_6$ (M = Sb, Bi). The computations of Pugh's ratio and Poisson's ratio of both halide shows their ductility, moreover, indirect band gaps of 0.1 eV/0.88 eV were obtained and considerable absorption coefficient was attained and therefore suggest the suitability for optoelectronic application [20–22]. Shah et al. explored the structural, phononic, electronic, electronic, and magnetic optical as well as the thermoelectric properties of vanadium-based Pb-free perovskite Cs_2NaVX_6 (X = Cl, Br, I) materials. The authors pointed out notable thermodynamic stability, high absorption coefficient as well as power conversion factors up to 4.671×10^{11} W/msk^2 which affirms the applicability of the studied materials towards the successful fabrication of optoelectronic devices [23]. So far, notable progress towards the enhancement of optoelectronic properties of various materials as candidates for perovskite solar applications has been reported, nonetheless, the optimum conversion efficiency, as well as conversion factors, are quite still low, possibly due to the complex nature of the inherent materials that constitute the device architecture, and hence the reason for more exploits and diversity in the approach of tuning various molecular properties. Herein, different levels of doping have been adopted to enhance the optoelectronic properties of $Cs_2Cu_xNa_{1-x}VCl_6$ toward the effective utilization as efficient perovskite materials. The structural, electronic, and thermoelectric materials have been considered to this end.

2. Calculation method

The DFT analysis was carried out via the Quantum Espresso software package (QE), where the requisite preliminary parameters, including kinetic cut-off energy, crystal systems, lattice constants, and the Brillouin zone grid, were appropriately considered. The electronic structure calculation has been carried out via density functional theory as it concerns plane waves and pseudopotentials with the pwscf module of the QE package, and the exchange-correlation energy was approximated using the Generalized Gradient Approximation (GGA) and PBE functional. Normal state scalar-relativistic pseudopotentials for the different atomic species were used in all calculations, treating explicitly the electronic configuration structures of the atoms involved Cs = [Xe], $6s^1$, Na = [Ne], $3s^1$, V = [Ar], 3 d^3, $4s^2$, Cl = [Ne], $3s^2$, $3p^5$, Cu = [Ar], 3 d^{10}, $4s^1$.

The structural and electronic properties of a unit cell of the considered perovskite, are sourced for in the cubic crystallographic phase [24–27]. In a bid to obtain the best geometric configuration for the crystal structure and discover its ground state energy, the Broyden–-Fletcher–Goldfarb–Shanno (BFGS) minimization technique to relax the atomic potentials was applied. A finer mesh of the K-point size was set at 12 × 12 x 12, represented by the Monkhorst-Park K-point scheme, and was utilized for all calculations. By emphasis, the cut-off energy value is projected from the partition of the valence and the core energy configurations. The cut-off energy value for particle density is 400 eV for the studied material. Following existing literature, the convergence criteria is fixed at the value 10^{-6} eV/atom [28]. Boltzmann transport theory was crucial in obtaining a thermoelectric response of the compounds by means of the BoltzTraP code [29].

3. Results and discussion

3.1. Structural and electronic properties

In accordance with the aforementioned information, the crystal structures of pure perovskite, and doped perovskite (at different levels) in this research were preferred to be the cubic framework, as shown in Fig. 1. The studied double perovskite usually denoted by the general formula $A_2BB'X_6$ belongs to the space group 225 (Fm3m). As such, the face centered cubic (FCC) crystal lattice structure $Cs_2Cu_xNa_1$-$xVCl_6$ represented by the formula where A, B, B′ designate transition and alkali metals respectively and X_6 designate halide ion occupies 8c, (0.25, 0.25 and 0.25), 4 b and 4a atom site while the halogen Cl assumes the 24e Wyckoff position respectively.

The equilibrium lattice parameter was calculated via Murnaghan's equation of state [30]. The detailed information with respect to the calculated lattice parameter as well as band gap which is found to have an inverse relationship with lattice parameter i.e. increase in the calculated lattice parameter is inversely proportional to the arithmetic digression observed at the band gap are carefully presented in Table 1. These observations correlate with the reported findings [31]. In addition, GGA + U value of the Hubbard-U parameter was optimally utilized so that the values of various parameters like band gaps to be more accurate. The figures of equilibrium lattice constant were reported since the energy minima of the studied perovskite are consistently affirming the stability of the optimized structures. Nevertheless, the Hubbard–U values were calculated using density functional perturbation theory (DFPT) embedded in the Quantum Espresso package [32–34] (see Table 1). Interestingly, the result obtained from the structural and electronic properties of $Cs_2Cu_xNa_{1-x}VCl_6$ divulged that the increase in percentage doping (25, 50, 75 and 100%) is directly proportional to the decrease in the band gap (1.71, 1.15, 1.14 and 1.12 eV) which suggests the efficaciousness of the material to possess a semiconducting potency. The band gap of 1.0–1.70eV permits the mobility of electrons without creating excess infrared rays and thus suggests the efficacy of the perovskite solar cell.

Table 1 gives the band gaps in the electron volts (eV) in accordance with the degree of doping. While Fig. 2 shows the band structure diagrams for this information. It therefore can be concluded that 100% doping or replacements of vanadium atoms by its copper counter parts is best suited for this perovskite material.

The equilibrium lattice constant in accordance with the percentage doping is presented in Table 1. From this information, it can be observed that the higher the percentage doping on the lattice, by the removal of vanadium atoms, the higher the equilibrium lattice constant i.e increase in percentage doping is directly proportional to the observed increase in equilibrium lattice of the perovskite material. These values have a range of 0.23, with a mean value of 10.59 between them. This shows larger spacing between the atoms on doping, making the lattice porous and softer and the softer material is the more stable and effective it is in solar

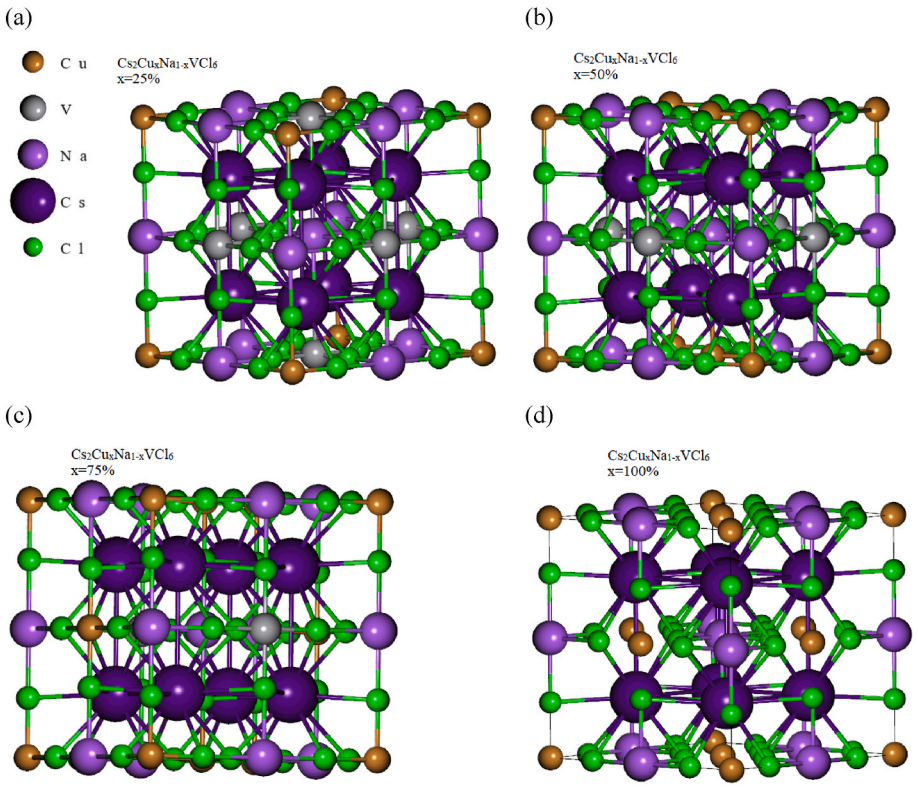

Fig. 1. Optimized geometry of the double perovskite materials studied.

Table 1
Band gaps of $Cs_2Cu_xNa_{1-x}VCl_6$.

Compound	Percentage of Cu (x in %)	DFT Functional	Band gap (eV)	Equilibrium Lattice constants (Å)
$Cs_2Cu_xNa_{1-x}VCl_6$	25	PBE	1.71	10.48
$Cs_2Cu_xNa_{1-x}VCl_6$	50	PBE	1.15	10.54
$Cs_2Cu_xNa_{1-x}VCl_6$	75	PBE	1.14	10.63
$Cs_2Cu_xNa_{1-x}VCl_6$	100	PBE	1.12	10.71

trapping. On the other hand, according to literature claims when the lattice constant increases with a corresponding decrease in the value of modulus of elasticity, there is a decrease in the stability of the perovskite material [35].Structurally, Continuous doping or replacement of the vanadium atoms on the perovskite material by copper atoms leads to better functioning and efficiency of the material which is observed to be less stable owing to the relationship between reported lattice constant and modulus of elasticity. Thus, it can be inferred that 25%of doping or replacements of Vanadium atoms by copper atoms give the best perovskite material [36].

3.2. Thermoelectric properties

The dimensionless figure of merit *ZT* is used to calculate a material's thermoelectric properties, which determines its energy conversion efficiency. An ideal thermoelectric material has high values of electrical conductivity and Seebeck coefficient while exhibiting low thermal conductivity value at the same time. The presence of dispersive bands and direct band gaps in $Cs_2Cu_xNa_{1-x}VCl_6$ allows the thermoelectric properties to be calculated. As such, material is expected to have large values of figure of merit (ZT). Thereby, better thermoelectric properties. Thermoelectric Figure merit (ZT) can be defined by the following equation (1).

$$ZT = \frac{S^2 \sigma T}{\kappa} \tag{1}$$

where σ is the electrical conductivity, S represents Seebeck coefficient, and κ represents thermal conductivity. Usually, electrons and phonons contribute towards total thermal conductivity. Although at higher temperature contribution from the lattice vibrations towards total thermal conductivity becomes less significant in comparison to electronic thermal conductivity [37]. This is due to the presence of a large flux of electrons at a higher temperature. Thereby, utilizing only electronic thermal conductivity for the calculation of thermoelectric figure of merit is decent approach [37–40]. Herein, we utilized BoltzTraP code which is based on Boltzmanntransport theory for the calculation of thermoelectric parameters. The BoltzTraP code estimates only the electronic part of the total thermal conductivity. Furthermore, electronic thermal and electrical conductivity was calculated per unit relaxation time. As seen from equation (1) thermoelectric figure of merit has the ratio of both parameters and hence becomes independent of relaxation time.

Plots of the electrical conductivity and the electronic contribution of thermal conductivity per unit relaxation time with respect to the temperature as well as graphs of Seebeck coefficient (S) and power factor (PF) are presented in Fig. 3 (a-d) for a temperature range of 100–800 K close to the Fermi level. Electrical conductivities are observed to increase with temperature having a maximum value of 0.16×10^{17}eV. It is also visible from Fig. 3 that electrical conductivities increase with respect to the doping percentage [41]. The decreasing pattern follows a trend as reported for band gap and lattice parameters. For temperatures between 100 and 800 K close to the Fermi level, the double perovskites, $Cs_2Cu_xNa_{1-x}VCl_6$, were doped with Cu at 25%, 50%, 75%, and 100% respectively. From Fig. 4 it is observed that the increase in temperature rises alongside the ZT value which is associated with an increase in

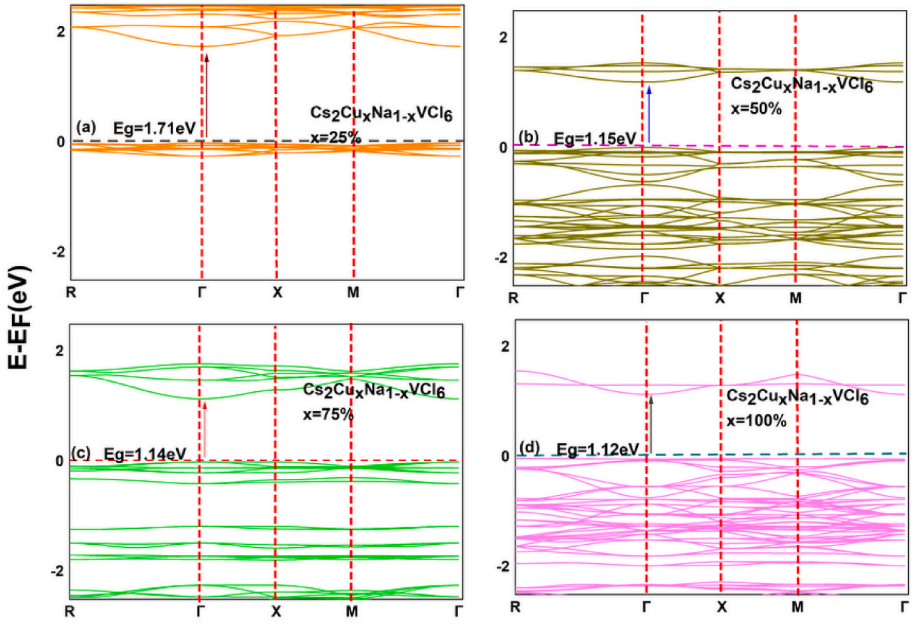

Fig. 2. The band structure of the compounds at 25%, 50%, 75%, and 100% level of copper doping on the perovskite $Cs_2Cu_xNa_{1-x}VCl_6$.

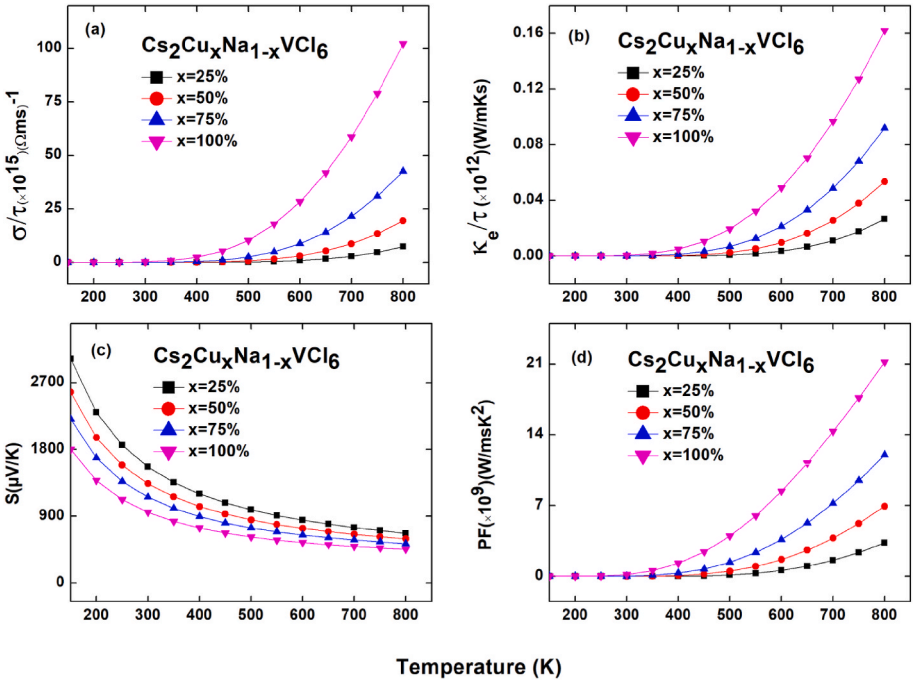

Fig. 3. Showing the graphs of different percentage of doping of copper on some electrical properties in tandem with temperature changes; (a) Electrical conductivity (b)Electronic thermal conductivity (c)Seebeck coefficients (d) Power factor: as analyzed from the perovskite material.

percentage doping for all the studied perovskite materials. From 0 K, the graph has a negative gradient until it gets to temperatures range between 440 K and 460 K where a gradual ascension was recorded until 800 K. Also, the result reveals that 50% and 75% doping are in phase after crossing the 500 K mark, but 100% doping was observed to deviate out of phase for all systems [42–45]. Overall, the values are in the order 25% < 50%<75% < 100% doping. The reason for this fall in the 25% doping and the second rise in the others is not farfetched. It is based on the closed-packed nature of the crystal lattice. As an increasing bond length is seen within the lattice on additional doping, the electrons have more space to move about, thereby increasing the entropy of the material in accordance with the second law of thermodynamics or universal law. It can also be seen that the band gap shows a decreasing pattern from 25% to 100%, and this trend has bearing on the figure of merit, by way of reducing the excitation energy required by the electrons [46]. The values close to or greater than unity is desired for thermoelectric power generation schemes [47–51].

4. Conclusion

This research has been tailored within the confines of a comprehensive and in-depth Density Functional Theoretical study and analysis

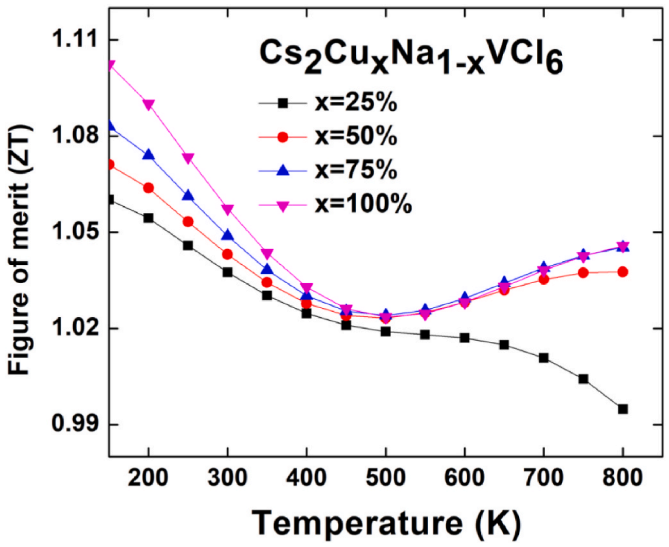

Fig. 4. Showing the graph of Thermoelectric Figure of merit (ZT) against Temperature (K).

on the structural, electronic, and thermoelectric properties of percentage doped Cu on Cs_2NaVCl_6 double perovskite. The obtained band gap parameter of 1.71–1.12 eV from the study confers the mobility of electrons at the perovskite material without creating excess infrared rays, affirming the efficacy of the system for thermoelectric application. In concordance with this, the electronic properties of the system suggest that continuous doping or replacement of the vanadium atom on the perovskite material by copper atom led to better functioning and efficacy of the material. Interestingly, the thermoelectric analysis reveals that the percentage doping follows a unique trend i.e 25% < 50% < 75% < 100% doping, as such the reason for this decreasing trend is based on the closed-packed nature of the crystal lattice. Also, an increase in bond length was observed within the lattice on additional percentage doping. As such, this observed change would create more space for electron mobility within the perovskite material, thereby, increasing the disorderliness (entropy) of the material, which in turn affirms correlates with the second law of thermodynamics or universal law. Thus, the increase in doping percentage increases the thermoelectric performance of the materials under study.

Funding

This work has not received funding from any agency or repository.

Declaration of competing interest

The authors declare that they have no known competing financial interests or personal relationships that could have appeared to influence the work reported in this paper.

Data availability

Data will be made available on request.

References

[1] M. Pazoki, M.B. Johansson, H. Zhu, P. Broqvist, T. Edvinsson, G. Boschloo, M. J. JohanssonE, Bismuth iodide perovskite materials for solar cell application: electronic structure, optical activity and directional charge transport. J, Phys. Chem. (2016).
[2] Q. Schiermeier, J. Tollefson, T. Scully, A. Witze, O. Morton, Electricity without Carbon. Nature 454 (2008) 816–823.
[3] M.M. Lee, J. Teuscher, T. Miyasaka, T.N. Murakami, H.J. Snaith, Efficient hybrid solar cells based on meso-SuperstructuredOrganometal halide perovskites, Science 338 (2012) 643–647.
[4] H.S. Kim, C.R. Lee, J.H. Im, K.B. Lee, T. Moehl, A. Marchioro, S.J. Moon, R. Humphry-Baker, J.H. Yum, J.E. Moser, et al., Lead iodide PerovskiteSensitizedAll-solid-state submicron thin film mesoscopic solar cell with efficiency Exceeding9%, Sci. Rep. 2 (2012) 591–597.
[5] M.A. Green, A. Ho-Baillie, H.J. Snaith, The emergence of perovskite solar cells, Nat. Photonics 8 (2014) 506–514.
[6] M. Grätzel, The light and shade of perovskite solar cells, Nat. Mater. 13 (2014) 838 (ACS Paragon Plus Environment. The Journal of Physical Chemistry).
[7] J. Bisquert, The swift surge of PerovskitePhotovoltaics, J. Phys. Chem. Lett. 4 (2013) 2597–2598.
[8] N.J. Jeon, J.H. Noh, Y.C. Kim, W.S. Yang, S. Ryu, S. Seok, Il. *Solvent Engineering for high-performance inorganic-organic hybrid perovskite solar cells*, Nat. Mater. 13 (2014) 897–903.
[9] H. Zhu, Y. Fu, F. Meng, X. Wu, Z. Gong, Q. Ding, M.V. Gustafsson, M.T. Trinh, S. Jin, X.Y. Zhu, Lead halide perovskite nanowire lasers with low lasing thresholds and high quality factors, Nat. Mater. 14 (2015) 636–642.
[10] H. Cho, S.H. Jeong, M.H. Park, Y.H. Kim, C. Wolf, C.L. Lee, J.H. Heo, A. Sadhanala, N. Myoung, S. Yoo, et al., Overcoming the ElectroluminescenceEfficiency limitations of perovskite light-emitting diodes, Science 350 (2015) 1222–1225.
[11] Z.K. Tan, R.S. Moghaddam, M.L. Lai, P. Docampo, R. Higler, F. Deschler, M. Price, A. Sadhanala, L.M. Pazos, D. Credgington, et al., Bright light-emitting diodes based on organometal halide perovskite, Nat. Nanotechnol. 9 (2014) 687–692.
[12] T. Leijtens, G.E. Eperon, N.K. Noel, S.N. Habisreutinger, A. Petrozza, H.J. Snaith, Stability of metal halide perovskite solar cells, Adv. Energy Mater. 5 (2015), 1500963.
[13] A. Babayigit, D. DuyThanh, A. Ethirajan, J. Manca, M. Muller, H.G. Boyen, B. Conings, Assessing the toxicity of Pb- and Sn-based perovskite solar cells in model organism DanioRerio, Sci. Rep. 6 (2016) 18721. Fabini, D. Quantifying the Potential for Lead Pollution from Halide PerovskitePhotovoltaics. J. Phys. Chem. Lett. 2015, 6, 3546–3548. Page 17 of 26ACS Paragon Plus Environment. The Journal of Physical Chemistry.
[14] M.R. Filip, F. Giustino, Steric engineering of metal-halide perovskites with tunable optical band gaps, Nat. Commun. 5 (2014) 5757.
[15] D.P. McMeekin, G. Sadoughi, W. Rehman, G.E. Eperon, M. Saliba, M.T. Horantner, A. Haghighirad, N. Sakai, L. Korte, B. Rech, et al., A mixed-cation lead MixedHalidePerovskite absorber for tandem solar cells, Science 351 (2016) 151–155.
[16] M. Pazoki, T.J. Jacobsson, A. Hagfeldt, G. Boschloo, Effect of metal CationReplacement on the electronic structure of metalorganic halide perovskites: replacement of lead with alkaline earth metals, Phys. Rev. B 93 (2016), 144105.
[17] N.K. Noel, S.D. Stranks, A. Abate, C. Wehrenfennig, S. Guarnera, A.A. Haghighirad, A. Sadhanala, G.E. Eperon, S.K. Pathak, M.B. Johnston, et al., Lead-free organic-inorganic tin halide perovskites for photovoltaic applications, Energy Environ. Sci. 7 (2014) 3061–3068.
[18] B.W. Park, B. Philippe, X. Zhang, H. Rensmo, G. Boschloo, E.M.J. Johansson, Bismuth based hybrid perovskites A3Bi2I9 (A: methylammonium or cesium) for solar cell application, Adv. Mater. 27 (2015) 6806–6813.
[19] R.L.Z. Hoye, R.E. Brandt, A. Osherov, V. Stevanovic, S.D. Stranks, M.W.B. Wilson, H. Kim, A.J. Akey, J.D. Perkins, R.C. Kurchin, et al., Methylammonium bismuth iodide as a lead-free, stable hybrid organic-inorganic solar absorber, Chem. Eur J. 22 (2016) 2605–2610.
[20] S. Idrissi, H. Labrim, L. Balmod, A. Benyoussef, DFT and TDDFT studies of the new inorganic perovskite CsPbI3 for solar cell applications, J. Chem. Phys. (2021). Elsevier.
[21] W. Zhang, G.E. Eperon, H.J. Snaith, Metal halide perovskites for energy applications, Nat. Energy 1 (2016), 16048.
[22] A. Swarnkar, et al., Quantum dot–induced phase stabilization of α-CsPbI3 perovskite for high-efficiency photovoltaics, Science 354 (2016) 92–95.
[23] W.J. Yin, T. Shi, Y. Yan, Unique properties of halide perovskites as possible origins of the superior solar cell performance, Adv. Mater. 26 (2014) 4653–4658.
[24] K. Marshall, et al., Enhanced stability and efficiency in hole-transport-layer-free CsSnI3 perovskitephotovoltaics, Nat. Energy 1 (2016), 16178.
[25] R.J. Sutton, et al., Bandgap-tunable cesium lead halide perovskites with high thermal stability for efficient solar cells, Adv. Energy Mater. 6 (2016), 1502458.
[26] J.B. Hoffman, A.L. Schleper, P.V. Kamat, Transformation of sintered CsPbBr 3 nanocrystals to cubic CsPbI3 and gradient CsPbBrxI3–x through halide exchange, J. Am. Chem. Soc. 138 (2016) 8603–8611.
[27] L.-Y. Huang, W.R. Lambrecht, Electronic band structure trends of perovskite halides: beyond Pb and Sn to Ge and Si, Phys. Rev. B 93 (2016), 195211.
[28] Q.A. Akkerman, et al., Strongly emissive perovskitenanocrystal inks for high-voltage solar cells, Nat. Energy 2 (2016), 16194.
[29] G.E. Eperon, et al., Inorganic caesium lead iodide perovskite solar cells, J. Mater. Chem. A 3 (2015) 19688–19695.
[30] T. Krishnamoorthy, et al., Lead-free germanium iodide perovskite materials for photovoltaic applications, J. Mater. Chem. A 3 (2015) 23829–23832.
[31] P. Ramasamy, et al., All-inorganic cesium lead halide perovskitenanocrystals for photodetector applications, Chem. Commun. 52 (2016) 2067–2070.
[32] N.R. Kumar, R. Radhakrishan, Optical properties of lead free perovskite Cs2InAg (BrxCl1-x)6 for solar cell applications: a DFT study, J. Mater Today: SAVE Proc. (2020).
[33] A. Kojima, K. Teshima, Y. Shirai, T. Miyasaka, Organometalic Halide perovskites as visible-light sensitizers for photovoltaic cells, J. Am. Chem. Soc. 131 (2009) 6050–6051.

[34] H.J. Snaith, Present status and future prospects of perovskitephotovoltaics, Nat. Mater. 17 (2018) 372–376.
[35] H. Fu, Review of Lead-free Hlaideperovskites as light absorbers for photovoltaic applications: from materials to solar cells, Sol. Energy Mater. Sol. Cells 193 (2019) 107–132.
[36] F. Giustino, H.J. Snaith, Toward lead-free perovskite solar cells, ACS Energy Lett. 1 (2016) 1233–1240.
[37] B. Saparov, et al., Thin film preparation and characterization of CS3Sb2I9 a lead-free layered perovskite semiconductor, Chem. Mater. 27 (2015) 5622–5632.
[38] W.A. Dunlap-Shohl, et al., Synthetic approach for halide perovskite thin films, Chem. Rev. 119 (2019) 3193–3295.
[39] C. Wu, et al., The dawn of lead perovskite solar cell: highly stable double perovskite Cs2AgBiBr6 film, Adv. Sci. 5 (2018), 1700759.
[40] V.K. Ravi, et al., Initiation and future prospects of colloidal metal halide double perovskitenanocrystals: Cs2AgBiX6 (X = Cl, Br, I), J. Mater. Chem. A 6 (2018) 21666–21675.
[41] N.R. Kumar, R. Radhakrishan, Electronic, optical, and mechanical properties of lead-free halide double perovskite using first principle density functional theory, Mater. Lett. 227 (2018) 289.
[42] S. Idrissi, H. Labrim, L. Balmod, A. Benyoussef, Study of the solar perovskite CsMBr3 (M = Pb or Ge) photovoltaic: band Gap engineering, Solid State Sci. 118 (2021), 106679.
[43] H. Zhu, M.T. Trinh, J. Wang, Y. Fu, P.P. Joshi, K. Miyata, S. Jin, X.Y. Zhu, Organic cations might not be essential to the remarkable properties of band edge carriers in lead halide perovskites, Adv. Mater. 29 (2017), 1603072.
[44] J. Song, J. Li, X. Li, L. Xu, Y. Dong, H. Zeng, Quantum dot light-emitting diodes based on inorganic perovskite cesium lead halides (CsPbX3), Adv. Mater. 27 (2015) 7162–7167.
[45] J. Song, J. Li, X. Li, L. Xu, Y. Dong, H. Zeng, Quantum dot light-emitting diodes based on inorganic perovskite cesium lead halides (CsPbX3), Adv. Mater. 27 (2015) 7162–7167.
[46] C.C. Stoumpos, C.D. Malliakas, J.A. Peters, Z. Liu, M. Sebastian, J. Im, T. C. Chasapis, A.C. Wibowo, D.Y. Chung, A.J. Freeman, et al., Crystal growth of the perovskite semiconductor CsPbBr3: a new material for high-energy radiation detection, Cryst. Growth Des. 13 (2013) 2722–2727.
[47] J. Deb, R. Mondal, S. Mukherjee, U. Sarkar, Thermoelectric properties of pentagraphene, Phys. B Condens. Matter 641 (2022), 414091.
[48] J. Deb, R. Mondal, U. Sarkar, H. Sadeghi, Thermoelectric properties of pristine graphyne and the BN-doped graphyne family, ACS Omega 6 (31) (2021) 20149–20157.
[49] R. Mondal, N.B. Singh, J. Deb, S. Mukherjee, U. Sarkar, Electronic and transport property of two-dimensional boron phosphide sheet, J. Mol. Graph. Model. 112 (2022), 1088117.
[50] J. Deb, D. Paul, Sarkar U. Pentagraphyne, A new carbon allotrope with the superior electronic and optical property, J. Mat. Chem. C. 8 (2020) 16143–16150.
[51] J. Deb, U. Sarkar, Boron-nitride and boron-phosphide doped twin-graphene: applications in electronics and optoelectronics, Appl. Surf. Sci. 541 (2021), 148657.